Computers and Fluids 181 (2019) 135–142

Contents lists available at ScienceDirect

Computers and Fluids

journal homepage: www.elsevier.com/locate/compfluid

Lattice Boltzmann study of effective viscosities of porous particle suspensions

Xuechao Liu, Haibo Huang*, Xi-Yun Lu

Department of Modern Mechanics, University of Science and Technology of China, Hefei, Anhui 230026, China

ARTICLE INFO

Article history:
Received 21 August 2018
Revised 7 December 2018
Accepted 8 January 2019
Available online 15 January 2019

Keywords:
Lattice Boltzmann method
Porous particle
Two-phase flow
Effective viscosities

ABSTRACT

The effective viscosities of dilute and semi-dilute suspensions in a two-dimensional shear flow are studied using the lattice Boltzmann method. The suspensions contain non-Brownian hard circular buoyant porous particles. Here a more accurate formula for intrinsic viscosity as a function of Darcy number (*Da*) for the whole *Da* regime is proposed through our numerical result. The effects of fluid inertia, permeability of the particle, and confinement of the bounding walls are investigated. It is found that for the cases with a small *Da*, the effective viscosity significantly increases with confinement and fluid inertia. However, for the cases with a large *Da*, the confinement ratio and fluid inertia have very minor effect. Moreover, for semi-dilute suspensions, the permeability of the particle weakens the effect of the hydrodynamic interactions between particles on the relative viscosity η_r and makes η_r decrease. The above phenomena can be well understood through quantifying the disturbance of the porous particle to the flow.

1. Introduction

Suspended or dispersed particles in a viscous liquid occur in widespread natural and man-made settings, for example, blood, proteins, paint, waste slurries. The viscosity of particle suspension is important in controlling industrial flow processes accurately [1]. A variety of theoretical, experimental and numerical studies have been carried out to understand the relative viscosity η_r of suspension, which is the ratio between effective viscosity of the suspension and viscosity of the pure fluid. In 1906, Einstein analytically studied the relative viscosity of dilute particle suspensions, where the hydrodynamic interactions between the particles are neglected. In his theory, the relative viscosity is $\eta_r = 1 + [\eta]\phi$, where ϕ is the solid volume fraction and intrinsic viscosity $[\eta] = \frac{5}{2}$ for hard spheres [2]. Later, Batchelor [3] theoretically extended this relationship to second order: $\eta_r = 1 + [\eta]\phi + \beta\phi^2$ where $\beta = 6.2$ for Brownian suspensions in any flow and $\beta = 7.6$ for non-Brownian suspensions in pure straining flow. For higher concentrated suspensions in which particle crowding causes hydrodynamic interactions among particles, Krieger and Dougherty [4] proposed the semi-empirical expression: $\eta_r = (1 - \frac{\phi}{\phi_m})^{-[\eta]\phi_m}$, where ϕ_m is the maximum packing concentration of particle, at which there is no fluid to lubricate relative particle motion any more. Recently, based on the work [5], Zhu et al. [6] proposed a simple parametric equation which describes the relative viscosity of a suspension as a function of suspended solid concentration, covering a wide range from very dilute to highly concentrated states.

In addition to the effect of the volume fraction of particles, the effects of the confinement ratio and inertia on the relative viscosity were also investigated. Davit and Peyla [7] found that the effective viscosity of suspensions in a shear flow between two walls changes abruptly with strong confinements. Fornari et al. [8] found that the suspension's effective viscosity decreases if the width of the channel is an integer multiple of particle diameter. Doyeux et al. [9] studied the confinement effect on η_r of the sheared two-dimensional suspensions of non-Brownian disks in the presence of walls. Lin et al. [10] studied the inertial effects on the suspension of hard sphere and proposed a formula for the suspension viscosity $\eta_r = 1 + (2.5 + 1.34Re^{1.5})\phi$, where $Re = \frac{\gamma D^2}{4\nu}$ and γ, D, and ν are shear rate, particle diameter, and kinematic viscosity, respectively. Furthermore, Lorenz et al. [11] studied the rheology of dense polydisperse frictional suspensions and Ye et al. [12] investigated the intrinsic viscosity of dilute non-spherical capsule suspension.

The main focus of the above studies have been on the viscosity of suspensions of impermeable particles. In reality, permeable particles are frequently encountered and are important in various fields of science and technology [13]. The effects of the permeability on the flow patterns and the overall drag coefficient have been studied [14–17]. Moreover, Li et al. [18] investigated the

* Corresponding author.
E-mail address: huanghb@ustc.edu.cn (H. Huang).

https://doi.org/10.1016/j.compfluid.2019.01.013
0045-7930/

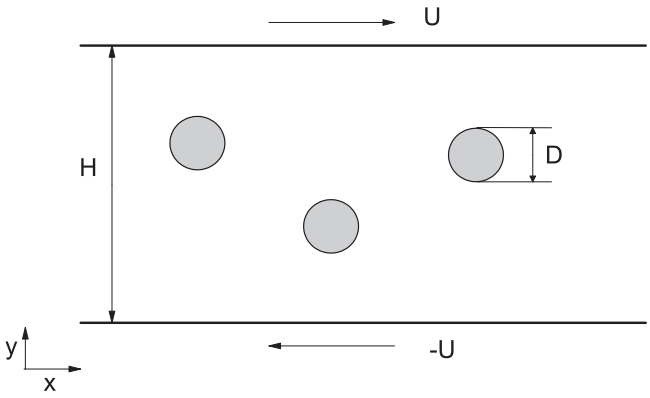

Fig. 1. Schematic diagram for particles moving in a shear flow.

rotational behavior of porous circular particle in shear flow. Recently, Xu et al. [19] studied the shear viscosity of porous particle suspensions. They found that the intrinsic viscosity changes nonlinearly at low *Da* regime but linearly at high *Da* regime, where $Da = \frac{K}{D^2}$, K is the permeability of particles and the intrinsic viscosity increases linearly with *Re*. However, the data in their result is limited. Meanwhile, they did not consider the effect of the confinement ratio and only the dilute suspensions were considered. Here we propose a more accurate formula for $[\eta]$ as a function of *Da* for the whole *Da* regime. Furthermore, the effects of confinement ratio and inertia are investigated and the semi-dilute cases are also considered.

For the numerical studies on suspension of porous particles, Darcy's law and the Brinkman equation are commonly used in the literature to describe the fluid flow within the permeable particle. For example, using Darcy's law, Burganos et al. [20] investigated the creeping flow around and through a permeable sphere, which is moving towards a solid planar wall. Using Brinkman equation, Roy and Damiano [21] studied the motion of a porous sphere in a stokes flow parallel to a planar confining boundary. However, using Darcy's law or the Brinkman equation is only valid for fluid flow with sufficient low *Re*, such as creeping flow. Recently, adopting the general volume-averaged conservation equations [22], Wang et al. [22] proposed a momentum equation to formulate the fluid flows around and through a permeable particle, which is more suitable for fluid flow with finite *Re*.

In this paper, we numerically investigate the relative viscosity of porous circular particle suspension in a two-dimensional shear flow using the momentum equation proposed by Wang et al. [22]. Here the Lattice Boltzmann method is used to solve the improved equations [22]. The numerical method is introduced in Section 2 and validated in Section 3. Results and discussion are presented in Section 4. Finally conclusions are addressed in Section 5.

2. Computational model

2.1. Governing equations

In this work we consider circular, neutrally buoyant, porous particles which undergoes translational and rotational motions in a simple shear flow as illustrated in Fig. 1. The fluid flow in a rectangular channel of Length L and width H is driven by two impermeable parallel plates moving in opposite direction with the same speed U. The shear rate is defined as $\gamma = \frac{2U}{H}$. There are three key dimensionless numbers: *Da*, the particle Reynolds number $Re_p = \frac{\gamma D^2}{\nu}$ and the confinement ratio $B = \frac{H}{D}$. In our simulations, for a dilute case there is only one particle in the computational domain. For a semi-dilute case, there are multiple particles inside the computational domain. It is noted that in all simulations, periodic boundaries are imposed in the x direction.

The volume-averaged macroscopic equations in terms of intrinsic phase-average is used to solve the fluid flow around and through the porous particle. The equations can be written as [22],

$$\frac{\partial \langle \boldsymbol{u}_f \rangle^f}{\partial t} + \langle \boldsymbol{u}_f \rangle^f \cdot \nabla \langle \boldsymbol{u}_f \rangle^f = -\frac{1}{\rho_f} \nabla \langle p_f \rangle^f + \nu \nabla^2 \langle \boldsymbol{u}_f \rangle^f + \boldsymbol{F}_m, \quad (1)$$

$$\nabla \cdot \langle \boldsymbol{u}_f \rangle^f = 0, \quad (2)$$

where ρ_f is the fluid density and $\langle \boldsymbol{u}_f \rangle^f$ and $\langle p_f \rangle^f$ are the intrinsic phase-average velocity and pressure of fluid phase, respectively [22]. $\boldsymbol{F}_m$ is the total body force

$$\boldsymbol{F}_m = -\frac{\varepsilon \nu}{K} (\langle \boldsymbol{u}_f \rangle^f - \langle \boldsymbol{u}_s \rangle^s) - \frac{\varepsilon^2 F_\varepsilon}{\sqrt{K}} (\langle \boldsymbol{u}_f \rangle^f - \langle \boldsymbol{u}_s \rangle^s) |\langle \boldsymbol{u}_f \rangle^f - \langle \boldsymbol{u}_s \rangle^s| + \boldsymbol{G}, \quad (3)$$

where $\langle \boldsymbol{u}_s \rangle^s$ is the intrinsic phase-average velocity of particle, and ε is the porosity of particle. $\boldsymbol{G}$ is the external force. The permeability K quantifies the ability of the porous particle to transmit fluids and geometric function F_ε of the porous medium is a function of ε [23]

$$K = \frac{\varepsilon^2 d_p^2}{150(1-\varepsilon)^2}, \quad (4)$$

$$F_\varepsilon = \frac{1.75}{\sqrt{150\varepsilon^3}}, \quad (5)$$

where d_p is the diameter of filling grains within the porous medium.

The flow in a moving porous medium is characterized by the porosity ε, Re_p and *Da*. In the limit of $\varepsilon = 0$, K approaches to zero and the porous particle reduces to a solid impermeable particle, whereas as ε approaches unity, the porous regime would be filled by fluid. Therefore, the macroscopic equations can be used for the whole domain with different values of ε in different regions. The translational and rotational motions of the particle are governed by Newtonian dynamics,

$$\boldsymbol{F} = M_p \frac{d\boldsymbol{U}_p}{dt}, \quad (6)$$

$$\boldsymbol{T}_p = I_p \frac{d\boldsymbol{\omega}_p}{dt}, \quad (7)$$

where $\boldsymbol{F}$ and $\boldsymbol{T}_p$ are the force and torque experienced by the particle, respectively. M_p is the particle mass, and I_p is the moment of inertia of particle. $\boldsymbol{U}_p$ and $\boldsymbol{\omega}_p$ are translational and rotational velocities of particle, respectively. The momentum-exchange method is adopted to calculate the force and torque exerted on the particle by the fluid [24]. When the gap between two particles is small, the lubrication force should be considered to avoid overlapping of particles. Based on the treatment [25], Kromkamp et al. [26] proposed the lubrication force for the two-dimensional system,

$$\boldsymbol{F}_{ij} = \begin{cases} -\frac{\nu \hat{\boldsymbol{R}}_{ij} \hat{\boldsymbol{R}}_{ij} \cdot \boldsymbol{U}_{ij}}{2} \left[\left(\frac{a_i + a_j}{h} \right)^{\frac{3}{2}} \left(F_0 + \frac{h}{a_i + a_j} F_1 \right) - \left(\frac{a_i + a_j}{h_c} \right)^{\frac{3}{2}} \left(F_0 + \frac{h_c}{a_i + a_j} F_1 \right) \right] & h < h_c \\ 0 & h > h_c \end{cases} \quad (8)$$

where F_0 is the numerical constant $\frac{3\pi\sqrt{2}}{4} = 3.3322$ and F_1 is the first order correction with a value of $\frac{231\pi\sqrt{2}}{80} = 12.829$. The unit vector $\hat{\boldsymbol{R}}_{ij} = \frac{\boldsymbol{R}_{ij}}{|\boldsymbol{R}_{ij}|}$, where $\boldsymbol{R}_{ij} = \boldsymbol{x}_i - \boldsymbol{x}_j$, $\boldsymbol{x}_i$ and $\boldsymbol{x}_j$ are positions of the

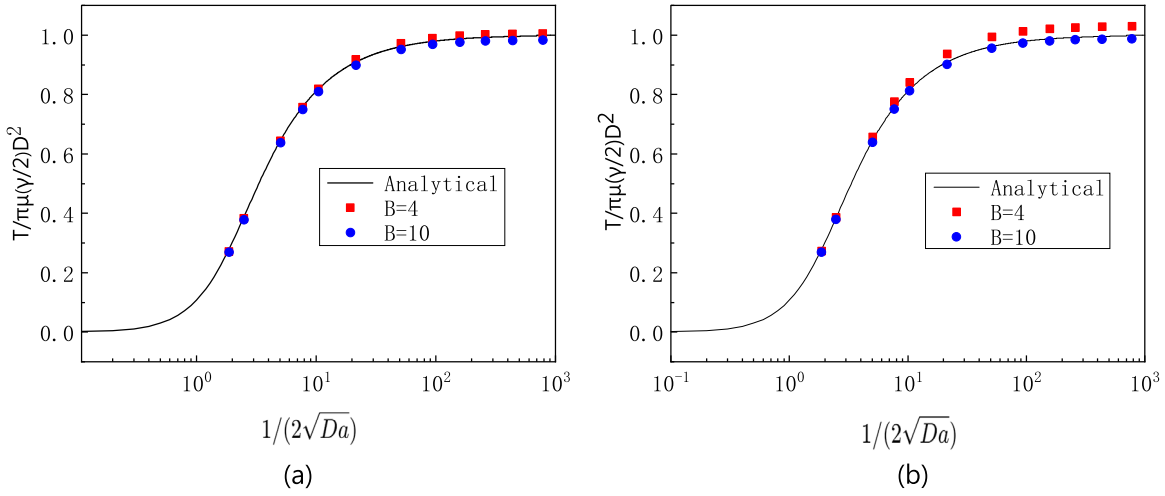

Fig. 2. Dimensionless torque acting on a porous particle as a function of $1/(2\sqrt{Da})$. (a) The particle is fixed in shear flow with shear rate γ; (b) the particle has no translational motion but rotates with angular velocity $\frac{\gamma}{2}$ in a quiescent fluid.

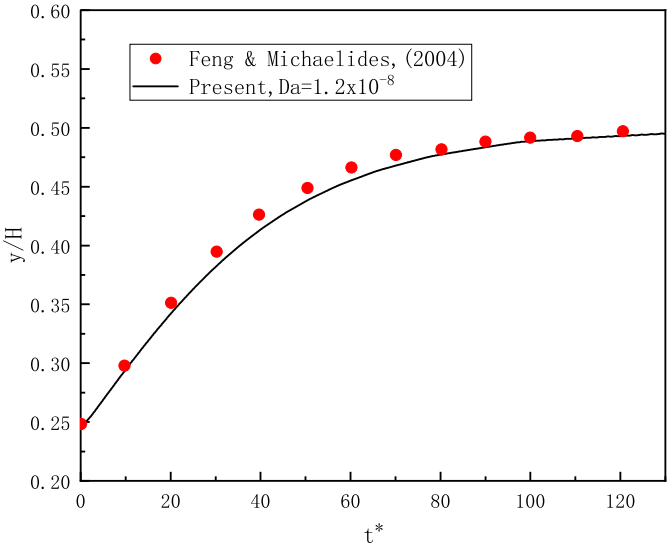

Fig. 3. The lateral migration of a particle in a shear flow.In the figure t^* is the non-dimensional time defined by $t* = \frac{TU}{H}$ where T is the time step.

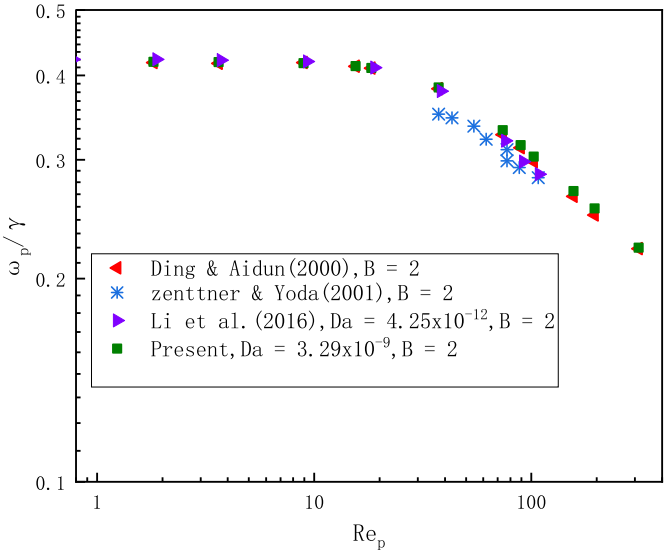

Fig. 4. Normalized rotational angular velocity ω_p/γ of a circular cylinder freely suspended in simple shear flow as a function of Re_p. Each square symbol denotes a case we simulated.

particle i and j, respectively. The particle's relative velocity is $\boldsymbol{U}_{ij} = \boldsymbol{U}_i - \boldsymbol{U}_j$. The gap distance between the particle $h = |\boldsymbol{R}_{ij}| - a_i - a_j$, where a_i and a_j denote the radii of the particle i and j. h_c is the cut-off distance.

2.2. Lattice Boltzmann method

The lattice Boltzmann method has become a particular useful tool to simulate particulate suspensions [24,25]. In this work the lattice Boltzmann is adopted to solve Eq. (1) and the evolution equation is

$$f_\alpha(\boldsymbol{x} + \boldsymbol{e}_\alpha \delta t, t + \delta t) - f_\alpha(\boldsymbol{x}, t) = -\frac{1}{\tau}[f_\alpha(\boldsymbol{x}, t) - f_\alpha^{eq}(\boldsymbol{x}, t)] + \delta t F_\alpha, \tag{9}$$

where τ is the relaxation time, $f_\alpha(\boldsymbol{x}, t)$ is the particle distribution function, $f_\alpha^{eq}(\boldsymbol{x}, t)$ is the equilibrium particle distribution function and F_α is the force term. $f_\alpha^{eq}(\boldsymbol{x}, t)$ and F_α are defined as

$$f_\alpha^{eq}(\boldsymbol{x}, t) = \rho_f \omega_\alpha [1 + \frac{\boldsymbol{e}_\alpha \cdot \boldsymbol{u}}{c_s^2} + \frac{(\boldsymbol{e}_\alpha \cdot \boldsymbol{u})^2}{2c_s^4} - \frac{\boldsymbol{u}^2}{2c_s^2}], \tag{10}$$

$$F_\alpha = \rho_f \omega_\alpha \left(1 - \frac{1}{2\tau}\right)\left[\frac{\boldsymbol{e}_\alpha \cdot \boldsymbol{F}_m}{c_s^2} + \frac{(\boldsymbol{e}_\alpha \cdot \boldsymbol{u})(\boldsymbol{e}_\alpha \cdot \boldsymbol{F}_m)}{c_s^4} - \frac{\boldsymbol{u} \cdot \boldsymbol{F}_m}{c_s^2}\right]. \tag{11}$$

In our LBM simulations, the D2Q9 velocity model is adopted. The discrete velocity $\boldsymbol{e}_\alpha$ is

$$\boldsymbol{e}_\alpha = \begin{cases} 0 & \alpha = 0 \\ c(cos[\frac{(\alpha-1)\pi}{4}], sin[\frac{(\alpha-1)\pi}{4}]) & \alpha = 1, 2, 3, 4 \\ \sqrt{2}c(cos[\frac{(\alpha-1)\pi}{4}], sin[\frac{(\alpha-1)\pi}{4}]) & \alpha = 5, 6, 7, 8 \end{cases} \tag{12}$$

The weighting parameters ω_α are defined as $\omega_\alpha = \frac{4}{9}$ for $\alpha = 0$, $\omega_\alpha = \frac{1}{9}$ for $\alpha = 1 - 4$, and $\omega_\alpha = \frac{1}{36}$ for $\alpha = 5 - 8$. The lattice speed c is given by $c = \frac{\delta x}{\delta t}$, where δx is the lattice size, and δt is the time step. $c_s = \frac{c}{\sqrt{3}}$ is the lattice sound speed. The macroscopic properties are related to the distribution functions by

$$\rho_f = \sum_{\alpha=0}^{8} f_\alpha, \rho_f \boldsymbol{u} = \sum e_\alpha f_\alpha + \frac{\delta t}{2} \rho_f \boldsymbol{F}_m. \tag{13}$$

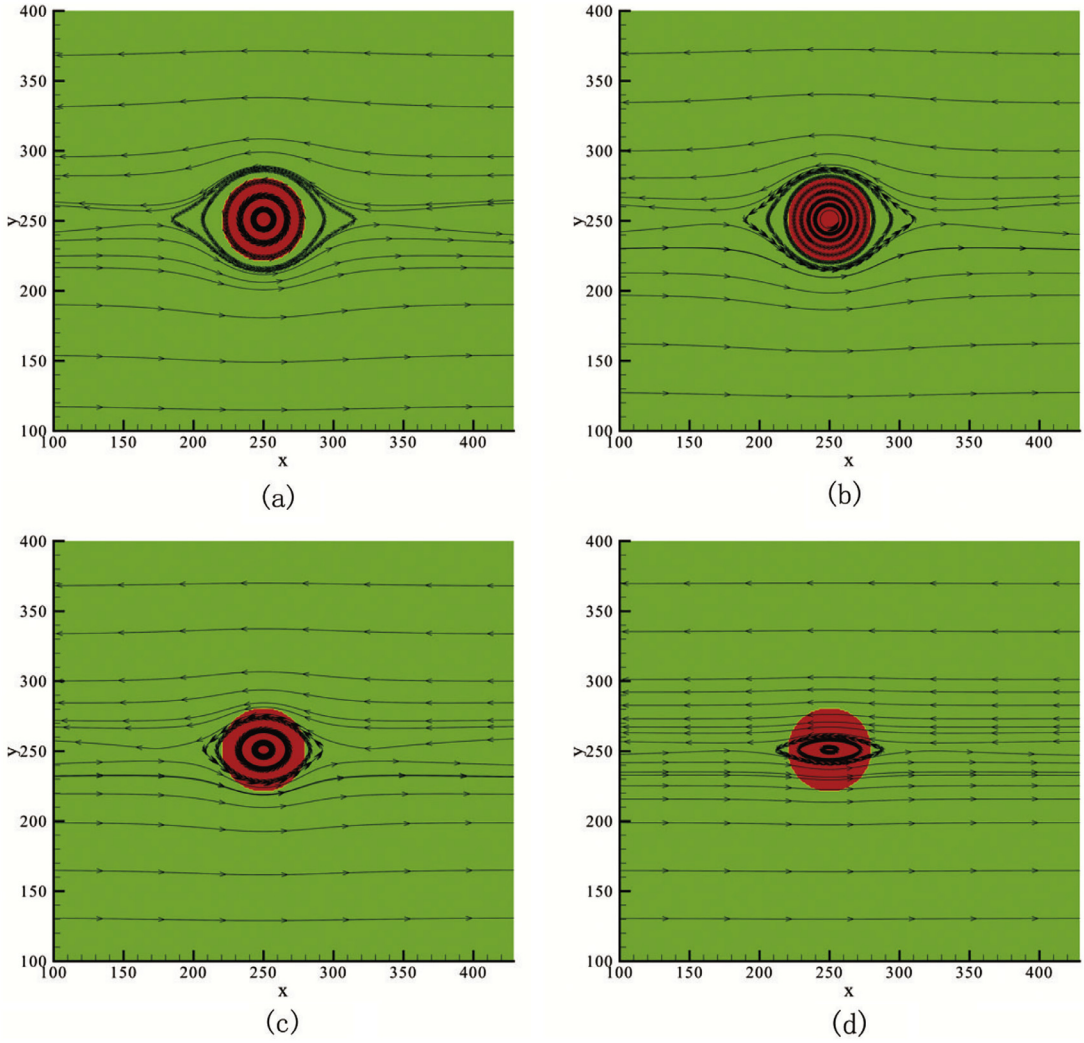

Fig. 5. Streamlines for a porous particle with different Da in shear flow, (a) $Da = 10^{-5}$, (b) $Da = 10^{-4}$, (c) $Da = 10^{-2}$, (d) $Da = 10^{-1}$.

By introducing (3) to (13), the macroscopic velocity is calculated as [22,27]

$$\boldsymbol{u} = \frac{\boldsymbol{v}}{d_0 + \sqrt{d_0^2 + d_1|\boldsymbol{v}|}} + \boldsymbol{u}_s, \tag{14}$$

where $\boldsymbol{u}_s = \boldsymbol{U}_p + \boldsymbol{\omega}_p \times (\boldsymbol{x} - \boldsymbol{x}_p)$ is velocity at a lattice node $\boldsymbol{x}$ inside the particle region and $\boldsymbol{x}_p$ is the position of the particle center. $\boldsymbol{v}$ is the temporal variable and is calculated by Guo and Zhao [27]

$$\boldsymbol{v} = \frac{1}{\rho_f}\sum_{\alpha=0}^{8} \boldsymbol{e}_\alpha f_\alpha + \frac{1}{2}\delta t \boldsymbol{G} - \boldsymbol{V}_p. \tag{15}$$

The two parameters d_0 and d_1 are $d_0 = \frac{1}{2}(1 + \frac{\delta t \varepsilon \nu}{2K})$, $d_1 = \frac{\delta t \varepsilon^2 F_\varepsilon}{2\sqrt{K}}$. The relative viscosity of the particle suspension in a shear flow is calculated by

$$\eta_r = \frac{\eta_{susp}}{\eta_f} = \frac{\sigma}{\rho \nu \gamma}, \tag{16}$$

where η_{susp} is the apparent viscosity of the particle suspension, which is calculated by $\eta_{susp} = \frac{\sigma}{\gamma}$. η_f is the viscosity of the solvent of the suspension which is calculated as $\eta_f = \rho\nu$. The average shear stress σ is obtained through averaging the shear stress acting on the moving flat walls over time. The periodic boundary conditions are implemented in the flow direction, and the extrapolation method is used for the impermeable parallel plates [28]. It is noted that in this method the boundary condition between the porous particle region and free flow is satisfied automatically [22].

3. Validation

To validate the numerical model, a test examining the torque exerted on a porous circular particle with small Re_p is performed. Two situations are considered, (a) the particle is fixed in shear flow with shear rate γ, and (b) the particle has no translational motion but rotates with an angular velocity $\omega = \frac{\gamma}{2}$ in a quiescent fluid. According to the theoretical work of Masoud et al. [29], the torque acting on a porous circular particle in a simple two-dimensional shear flow with the shear rate γ is

$$T = -\frac{\pi \mu \gamma D^2}{2} \frac{I_2\left(\frac{1}{\sqrt{4Da}}\right)}{I_0\left(\frac{1}{\sqrt{4Da}}\right)}, \tag{17}$$

where T is the magnitude of the torque, and I_2 and I_0 are modified Bessel functions of the first kind. μ is the dynamic viscosity. In the simulation, the particle Reynolds number is set to be $Re_p = 0.01$. The density of the fluid and the particle are identical and Da

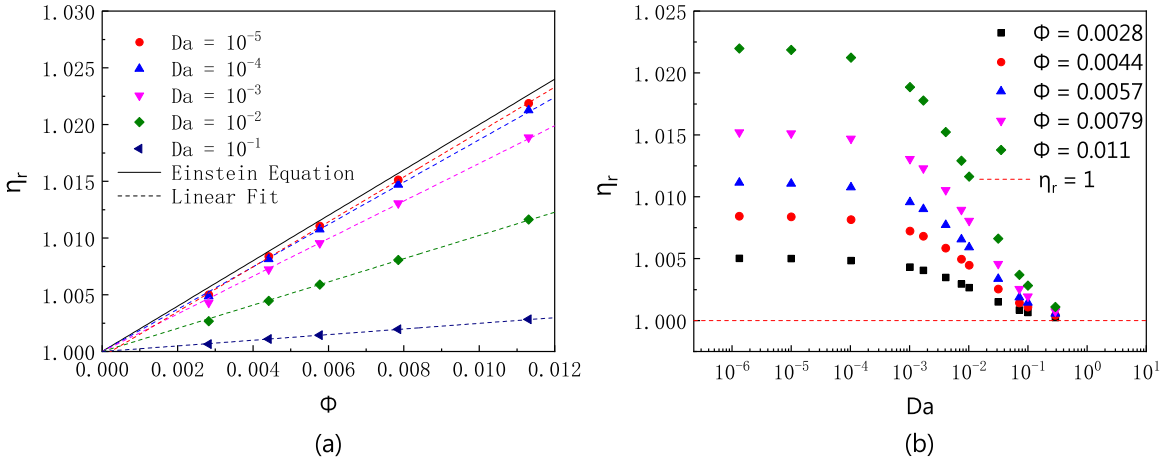

Fig. 6. Relative viscosity η_r (a) as a function of the volume fraction ϕ for various Da, the black solid line is the results for solid impermeable particle, the dash line is the linear fit of the simulation results, and (b) as a function of Da for various ϕ.

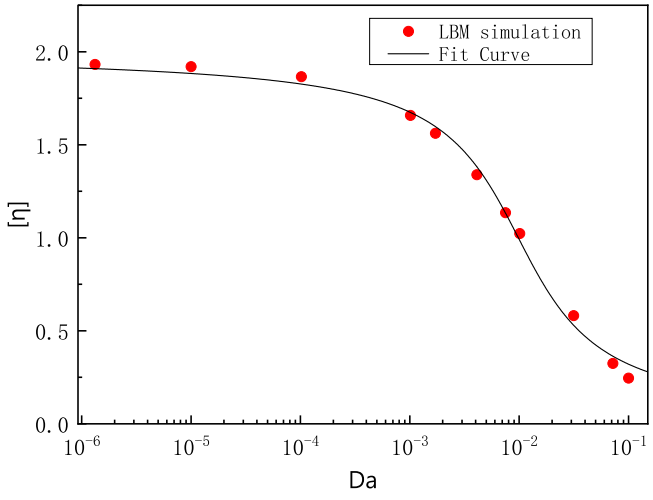

Fig. 7. The intrinsic viscosity $[\eta]$ as the function of Da.

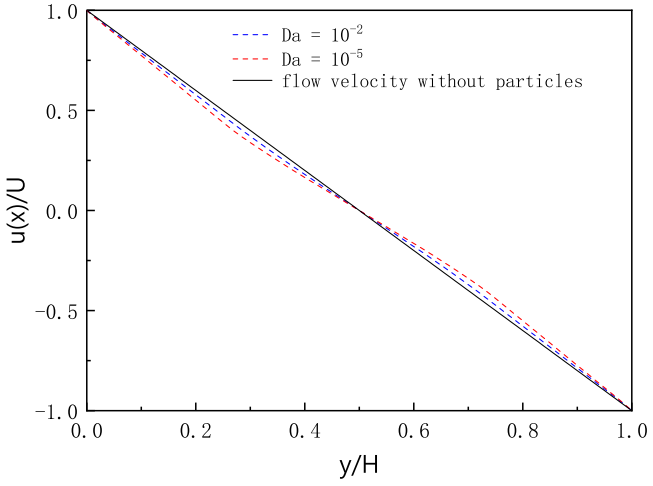

Fig. 8. The dimensionless time-averaged axial velocity with $Da = 10^{-2}$ and $Da = 10^{-5}$. The solid line is the dimensionless velocity for pure fluid in shear flow.

varies from 10^{-7} to 10^{-2}. Confinement ratios $B = 4$ and $B = 10$ are considered.

Fig. 2 shows our results of normalized torque on the porous particle and those of the analytical solutions. We can see that the simulation results of $B = 10$ agree well with the analytical results and the results of $B = 4$ have a very small deviation. The results validate our numerical method. It is also seen that the confinement ratio, which is not considered in the analytical solution, has an influence on the particle dynamics.

Next, the benchmark problem of a neutrally buoyant two-dimensional porous particle moving in shear flow between two plates is tested. The parameters used in the simulation are presented as follows: the plate width $L = 2000$, the height $H = 80$, the relaxation time $\tau = 0.6$, the diameter of particle $D = 20$, the Darcy number $Da = 1.2 \times 10^{-8}$. The two plates are moving with $U = 1/120$ in opposite directions. Initially the particle is at rest and placed at the position $y_0 = 0.25H$ above the bottom plate. The lateral migration of the particle is shown in Fig. 3. From the figure it is seen that evolution of lateral position obtained from present method agrees well with that of an impermeable particle in [30].

To further validate the method, the rotation of a porous circular cylinder freely suspended in simple shear flow is simulated. In this simulation, the computational domain has width $L = 600$ and height $H = 100$. The diameter of particle is $D = 50$. The corresponding confinement ratio is $B = 2$. The porous circular cylinder we simulated has a very small Darcy number $Da = 3.29 \times 10^{-9}$, which approximates its rigid impermeable counterpart. Normalized rotational angular velocity ω_p/γ of the cylinder as a function of Re_p is shown in Fig. 4. It is seen that the present result is consistent with the results in [18,31,32]. Hence, the present method is able to capture the inertial and confinement effects accurately.

4. Results and discussions

We consider one porous particle freely moving in a shear flow between two bounding walls. Here the volume fraction of particle (ϕ) is smaller than 0.012, and the effects of Da, B and Re_p on η_r are considered. In the simulations, the relaxation time is $\tau = 0.8$. Parameter ranges $Da \in (10^{-6}, 0.3)$, $\phi \in (0.0028, 0.011)$, $B \in (2, 12)$ and $Re_p \in (0.01, 6)$ are considered. The flow field inside and around the porous particle at $Da = 10^{-5}, 10^{-4}, 10^{-2}$ and 10^{-1} is shown in Fig. 5. It is seen that the penetration of the streamlines through the porous particle is prominent at a higher Da, e.g., $Da = 10^{-1}$, while the penetration is very weak at a lower Da, e.g., $Da = 10^{-5}$.

First only effect of Da on the relative viscosity of porous particle suspension is investigated. In these cases the effect of $B(B > 8)$ is negligible because the channel is wide enough. Re_p is fixed to be 0.01. Fig. 6 shows η_r as a function of the volume fraction ϕ and Da.

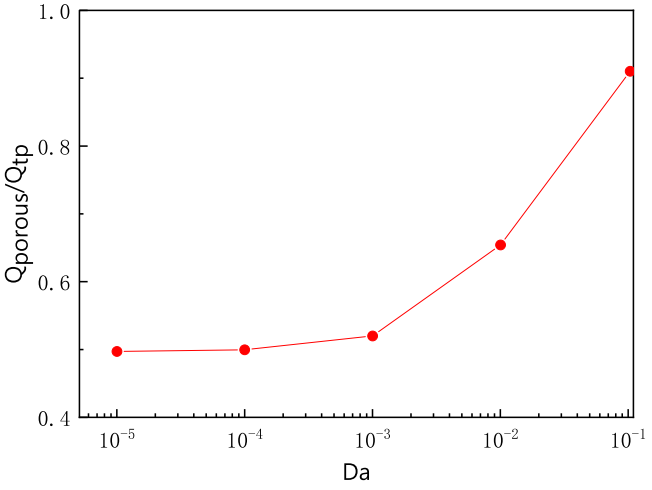

Fig. 9. The dimensionless flow rate as a function of *Da*. Q_{porous} is normalized by Q_{tp}, which is the flow rate in Eq. (19) without particle or that at infinite *Da*.

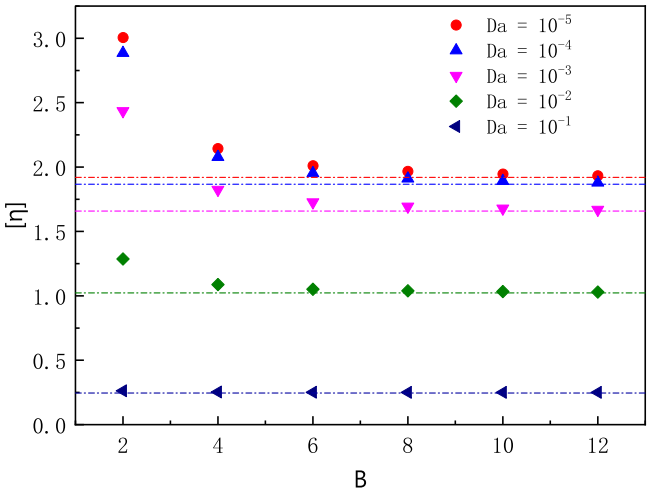

Fig. 10. The intrinsic viscosity $[\eta]$ as a function of *B*.The dash-dotted lines are drawn to guide the eye.

For different *Da*, η_r increases linearly with the increase of ϕ, which is similar with the dilute impermeable particle suspension. Linear fits of our numerical data are presented in Fig. 6(*a*). It is seen the slope of the linear fit decreases with *Da*. As *Da* approaches to zero, the particle becomes solid and impermeable. Hence, at a small *Da*, e.g., $Da = 10^{-5}$, the linear fit for η_r is close to that of the Einstein equation [2], which is derived from the solid impermeable particle suspension.

For a large *Da*, Fig. 6(*b*) shows that η_r decreases rapidly with an increasing *Da* when $Da > 10^{-3}$ and η_r decreases more rapidly for cases with higher ϕ. For a very large *Da*, e.g., $Da = 10^{-1}$, permeability of the particle is high and the presence of the particle has a minor effect on the shear flow, therefore the relative viscosity approaches to unity.

Fig. 7 shows the intrinsic viscosity $[\eta]$ as a function of *Da*. The results in Fig. 7 are similar to the result in Xu et al. [19] However, here a more accurate formula to fit the data points is proposed, i.e.,

$$[\eta] = 1 + \frac{2}{\pi}\arctan(a_1 + a_2\log(Da)), \tag{18}$$

where the two parameters a_1 and a_2 are $a_1 = -3.6 \pm 0.23, a_2 = -1.8 \pm 0.1$.

From Fig. 7, it is seen that when *Da* is close to zero, the intrinsic viscosity approaches 2 and when *Da* is infinite, the intrinsic viscosity approaches zero. However, data fitting in Xu et al. [19] does not have these features. Hence, here "more accurate" means that our formula is more consistent with physics. It is not due to only one formula or it covering the whole *Da* regime. From Fig. 7 we can also see that $[\eta]$ decreases with an increasing *Da*, indicating that the permeability of the particle reduces the effect of the particle on the fluid. Fig. 8 shows the normalized axial velocity profile ($U(x)/U$, where U is the velocity of the wall), which is averaged over one period. The discrepancy between the velocity profile of the suspension flow and that of the undisturbed fluid flow (without particle) quantifies the disturbance of the particle to the fluid. It is seen from Fig. 8 that the presence of porous particles with larger *Da* has a minor disturbance on the fluid flow, which is consistent with our intuition.

Usually, flow rate is also used to the quantify the disturbance to the flow. Suppose the center of the channel in the *y*-direction is $y = 0$, the flow rate passing the top-half of the particle due to permeability of the particle is defined as

$$Q_{porous} = \int_0^{\frac{D}{2}} u(x)dy \approx \frac{u_{ave}D}{2}, \tag{19}$$

where u is the fluid velocity and u_{ave} denotes the average fluid velocity along the top radius in the y direction of the particle [18]. It is noted that in the shear flow, the equilibrium position of a neutrally buoyant particle is $y = 0$. Q_{porous} as a function of *Da* is shown in Fig. 9. For $Da < 10^{-3}$, the flow rate increases very slowly with the increase of *Da*, whereas for $Da > 10^{-3}$, the flow rate increases dramatically. A larger Q_{porous} represents a smaller disturbance to the flow. Hence, variation of Q_{porous} also plausibly explains the results in Fig. 7 that $[\eta]$ changes slowly for small *Da* ($Da < 10^{-3}$) and drops quickly for large *Da* ($Da > 10^{-3}$).

For dilute and semi-dilute impermeable particle suspensions, the confinement ratio has a strong effect on η_r [7]. For a porous particle, the effect of B is investigated here. The intrinsic viscosity $[\eta]$ as a function of B is shown in Fig. 10. For a small *Da* ($Da \leq 10^{-2}$), the walls with strong confinements have non-negligible effect on the intrinsic viscosity. However, the influence of walls can be neglected for a large $Da(Da \geq 10^{-1})$. For a wide enough channel ($B > 8$), the walls have little influence on $[\eta]$ for any *Da*. Therefore, a critical B^* can be defined to illustrate the importance of the effect of confinement ratios. For $B > B^*$, $[\eta]$ remains almost constant with an increasing B, while for $B < B^*$, $[\eta]$ increases rapidly with a decreasing B. From Fig. 10, we identify that $B^* = 8$ for $Da = 10^{-5}$ and $B^* = 6$ for $Da = 10^{-2}$, which suggests that B^* decreases with an increasing *Da*.

To better understand the effect of the porous particle to the flow field, we plot the dissipation density field and the disturbance flow generated by the presence of the porous particle, which are shown in Fig. 11. The disturbance flow is obtained through the actual flow field subtracting the imposed shear flow. The dissipation density is obtained by Doyeux et al. [9]

$$\delta = \frac{1}{2}\rho\nu \mid \nabla\boldsymbol{u} + \nabla\boldsymbol{u}^T \mid^2 . \tag{20}$$

It is seen that the disturbance flows for $Da = 10^{-5}$ and $Da = 10^{-2}$ are similar. A discrepancy is that the magnitude of the dissipation for $Da = 10^{-2}$ is smaller than that of $Da = 10^{-5}$. Hence, the porous particle with a larger *Da* has smaller disturbance to the shear flow. That contributes to the results in Fig. 7, i.e., η_r decreasing with *Da*.

Next we consider the effect of particle Reynolds number on η_r. First the effect of walls is eliminated because $B > 8$ is chosen and $\phi = 0.00589$ is fixed. The relative viscosity η_r as a function of Re_p and *Da* is shown in Fig. 12(*a*). It is seen that the effect of Re_p can be neglected for $Re_p < 0.1$ and when $Re_p > 0.1$, η_r increases with an

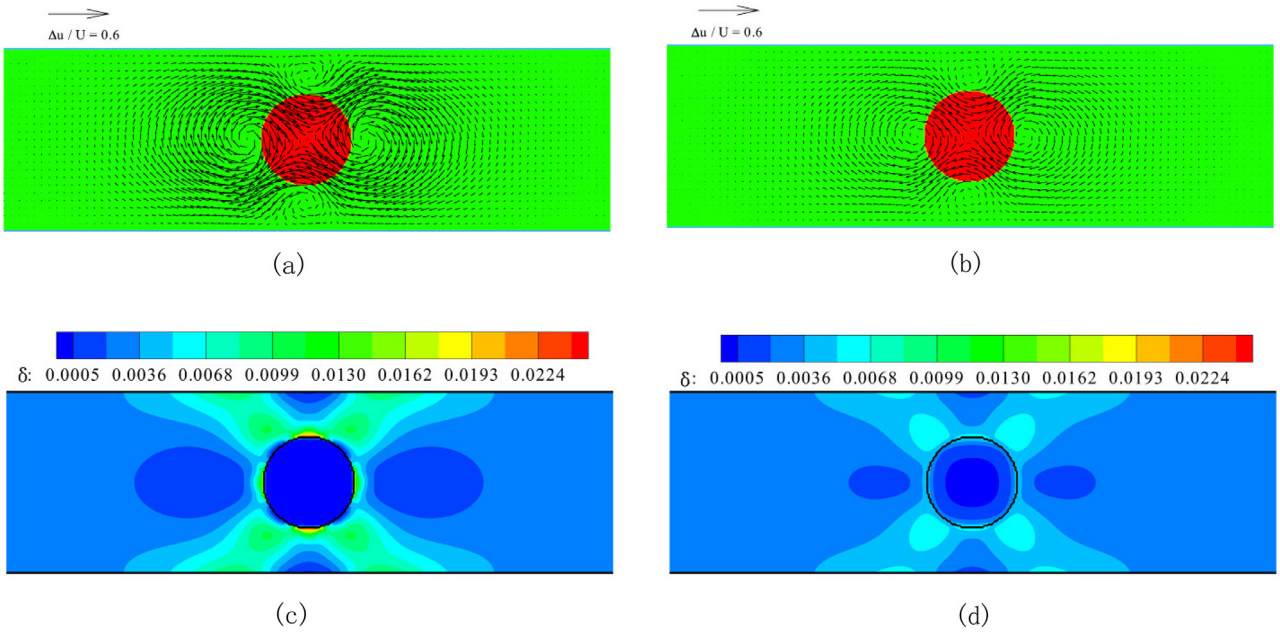

Fig. 11. The disturbance flow for (a) $Da = 10^{-5}$, (b) $Da = 10^{-2}$. The dissipation density field for (c) $Da = 10^{-5}$, (d) $Da = 10^{-2}$.

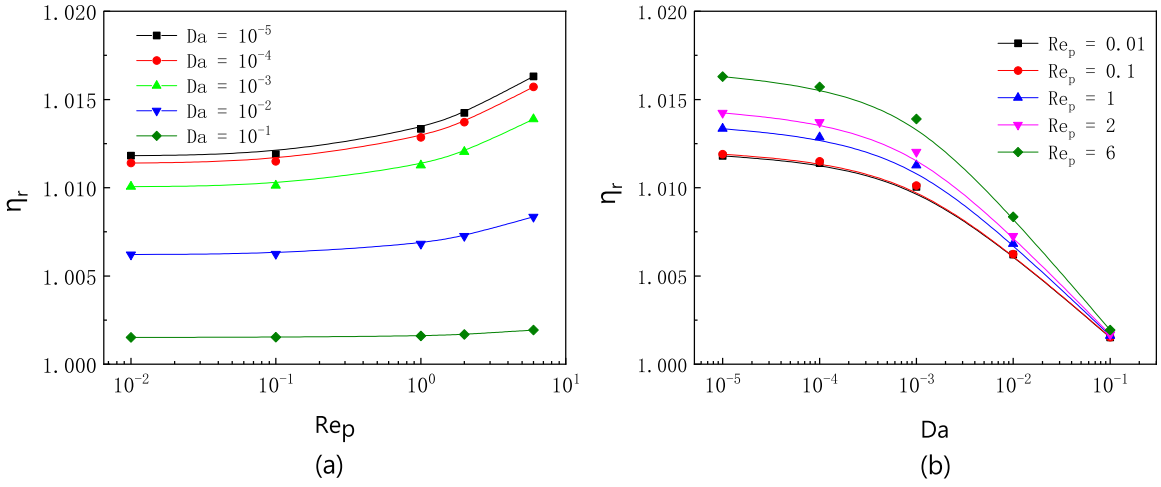

Fig. 12. The relative viscosity η_r (a) as a function of Re_p and (b) as a function of Da.

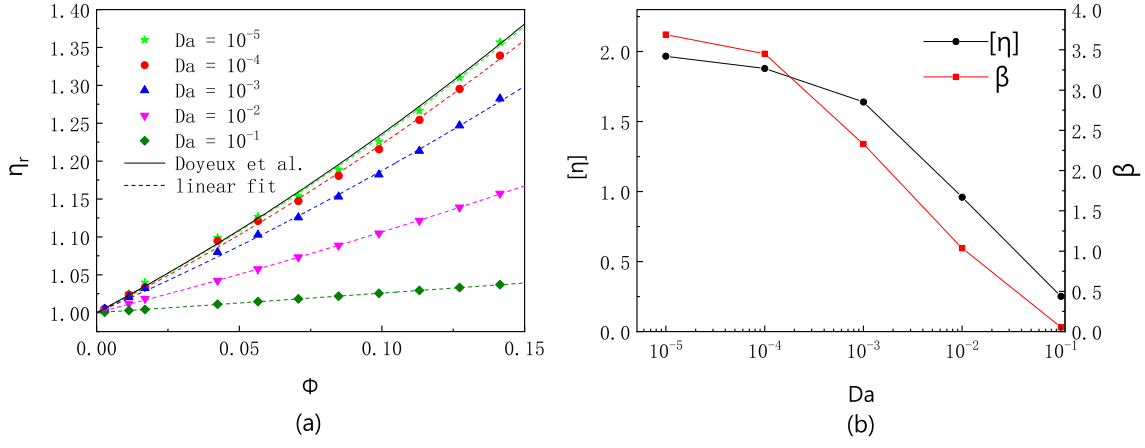

Fig. 13. (a) The relative viscosity as a function of ϕ, (b) intrinsic viscosity as a function of Da.

increasing Re_p. Fig. 12(b) shows that for different Re_p, η_r decreases with an increasing Da.

When the contribution of hydrodynamic interactions between particles are considered, the Einstein's calculations is expanded to second order [2,3]. Doyeux et al. [9] proposed the two-dimensional form

$$\eta_r = 1 + 2\phi + 3.6\phi^2. \tag{21}$$

Here, we also consider porous particles with a semi-dilute volume fraction ($\phi < 0.15$) in a simple shear flow, and the results are presented in Fig. 13(a). A seconder order function $\eta_r = 1 + [\eta]\phi + \beta\phi^2$ is adopted to fit the simulation data, and the results are shown in Fig. 13(b). The intrinsic viscosity $[\eta]$ decreases with an increasing Da, which is similar with the results of dilute suspension. Moreover, the value of β also decreases with Da. Because β value represents the effect of hydrodynamic interactions between particles on η_r, the result illustrates that the permeability of the porous particles also weakens the effect of hydrodynamic interactions between particles on η_r.

5. Conclusion

In this work, we have studied the effect of the Darcy number (Da), the confinement ratios (B) and the Reynolds number(Re_p) on the viscosity of the circular porous particle suspensions in a simple shear flow between two impermeable walls. The numerical simulations are performed using the model proposed by Wang et al. [22] and the lattice Boltzmann method is used to solve the fluid flow. The relative viscosities of dilute porous particle suspensions with parameter ranges $10^{-6} \le Da \le 0.3$, $2 \le B \le 12$ and $0.01 \le Re_p \le 6$ are investigated.

It is found that the correlation between η_r and ϕ for different Da is similar to that for a suspension of solid impermeable particles. It is identified that as Da increases, the particle disturbance to the shear flow decreases, which lead to the decrease of η_r. In addition, an accurate formula is proposed to describe the correlation between intrinsic viscosity and Da. For the confinement effect, the walls have significant effect on η_r when B is small. However, the effect of B is diminished as Da is large. The inertial effect at a large Re_p has significant effect on η_r, while the inertial effect is diminished as Da is large. For semi-dilute suspensions, it is found that the permeability of the porous particles weakens the effect of hydrodynamic interactions between particles on η_r.

The results of this paper may be helpful for understanding the effect of the permeability of particles in the suspension on its relative viscosity and may shed some light on the three-dimensional cases. On the other hand, this study is a two-dimensional work. Three-dimensional simulations will be performed to obtain more accurate quantitative results in the near future.

Acknowledgment

Huang is supported by National Natural Science Foundation of China (Grant nos. 11772326 and 11472269).

References

[1] Stickel JJ, Powell RL. Fluid mechanics and rheology of dense suspensions. Annu Rev Fluid Mech 2005;37:129–49.
[2] Einstein A. Eine neue bestimmung der moleküldimensionen. Ann Phys 1906;324(2):289–306.
[3] Batchelor G. The effect of Brownian motion on the bulk stress in a suspension of spherical particles. J Fluid Mech 1977;83(1):97–117.
[4] Krieger IM, Dougherty TJ. A mechanism for non-Newtonian flow in suspensions of rigid spheres. Trans Soc Rheol 1959;3(1):137–52.
[5] Quemada D, Berli C. Energy of interaction in colloids and its implications in rheological modeling. Adv Colloid Interface Sci 2002;98(1):51–85.
[6] Zhu Z, Wang H, Peng D. Dependence of sediment suspension viscosity on solid concentration: a simple general equation. Water (Basel) 2017;9(7):474.
[7] Davit Y, Peyla P. Intriguing viscosity effects in confined suspensions: a numerical study. Europhys Lett 2008;83(6):64001.
[8] Fornari W, Brandt L, Chaudhuri P, Lopez CU, Mitra D, Picano F. Rheology of confined non-Brownian suspensions. Phys Rev lett 2016;116(1):018301.
[9] Doyeux V, Priem S, Jibuti L, Farutin A, Ismail M, Peyla P. Effective viscosity of two-dimensional suspensions: confinement effects. Phys Rev Fluids 2016;1(4):043301.
[10] Lin CJ, Peery JH, Schowalter WR. Simple shear flow round a rigid sphere: inertial effects and suspension rheology. J Fluid Mech 1970;44(1):1–17.
[11] Lorenz E, Sivadasan V, Bonn D, Hoekstra AG. Combined lattice-Boltzmann and rigid-body method for simulations of shear-thickening dense suspensions of hard particles. Comput Fluids 2018;172:474–82.
[12] Ye H, Huang H, Sui Y, Lu X-Y. Dynamics of a nonspherical capsule in general flow. Comput Fluids 2016;134:31–40.
[13] Masoud H, Bingham BI, Alexeev A. Designing maneuverable micro-swimmers actuated by responsive gel. Soft Matt 2012;8(34):8944–51.
[14] Yu P, Zeng Y, Lee TS, Chen XB, Low HT. Steady flow around and through a permeable circular cylinder. Comput Fluids 2011;42(1):1–12.
[15] Zhu Q, Chen Y, Yu H. Numerical simulation of the flow around and through a hygroscopic porous circular cylinder. Comput Fluids 2014;92:188–98.
[16] Yu P, Zeng Y, Lee TS, Chen XB, Low HT. Numerical simulation on steady flow around and through a porous sphere. Int J Heat Fluid Flow 2012;36:142–52.
[17] Yu P, Zeng Y, Lee T, Bai H, Low H. Wake structure for flow past and through a porous square cylinder. Int J Heat Fluid Flow 2010;31(2):141–53.
[18] Li C, Ye M, Liu Z. On the rotation of a circular porous particle in 2d simple shear flow with fluid inertia. J Fluid Mech 2016;808:R3.
[19] Xu A, Shi L, Zhao T. Lattice Boltzmann simulation of shear viscosity of suspensions containing porous particles. Int J Heat Mass Transfer 2018;116:969–76.
[20] Burganos VN, Michalopoulou AC, Dassios G, Payatakes AC. Creeping flow around and through a permeable sphere moving with constant velocity towards a solid wall. Chem Engng Commun 1987;58(1–6):119–38.
[21] Roy B, Damiano E. On the motion of a porous sphere in a stokes flow parallel to a planar confining boundary. J Fluid Mech 2008;606:75–104.
[22] Wang L, Wang L-P, Guo Z, Mi J. Volume-averaged macroscopic equation for fluid flow in moving porous media. Int J Heat Mass Transfer 2015;82:357–68.
[23] Ergun S. Fluid flow through packed columns. Chem Engng Prog 1952;48(2):89–94.
[24] Aidun CK, Lu Y, Ding E-J. Direct analysis of particulate suspensions with inertia using the discrete Boltzmann equation. J Fluid Mech 1998;373:287–311.
[25] Ladd A, Verberg R. Lattice-boltzmann simulations of particle-fluid suspensions. J Stat Phys 2001;104(5–6):1191–251.
[26] Kromkamp J, Van Den Ende DT, Kandhai D, Van Der Sman RG, Boom RM. Shear-induced self-diffusion and microstructure in non-Brownian suspensions at non-zero Reynolds numbers. J Fluid Mech 2005;529:253–78.
[27] Guo Z, Zhao T. Lattice boltzmann model for incompressible flows through porous media. Phys Rev E 2002;66(3):036304.
[28] Guo Z, Zheng C, Shi B. An extrapolation method for boundary conditions in lattice Boltzmann method. Phys Fluids 2002;14(6):2007–10.
[29] Masoud H, Stone HA, Shelley MJ. On the rotation of porous ellipsoids in simple shear flows. J Fluid Mech 2013;733:R6.
[30] Feng Z-G, Michaelides EE. The immersed boundary-lattice Boltzmann method for solving fluid–particles interaction problems. J Comput Phys 2004;195(2):602–28.
[31] Ding E-J, Aidun CK. The dynamics and scaling law for particles suspended in shear flow with inertia. J Fluid Mech 2000;423:317–44.
[32] Zettner C, Yoda M. The circular cylinder in simple shear at moderate Reynolds numbers: an experimental study. Exp Fluids 2001;30(3):346–53.